Human Molecular Genetics, 2009, Vol. 18, No. 4 ***723–736***
doi:10.1093/hmg/ddn403
Advance Access published on November 27, 2008

Severe neurological phenotypes of Q129 DRPLA transgenic mice serendipitously created by *en masse* expansion of CAG repeats in Q76 DRPLA mice

Toshiya Sato[1], Masami Miura[5], Mitsunori Yamada[2], Takayuki Yoshida[6,†], Jonathan D. Wood[7,‡], Ikuru Yazawa[10], Masao Masuda[5], Takeo Suzuki[5,11], Ryong-Moon Shin[5,¶], Hau-Jie Yau[12], Fu-Chin Liu[12], Takayoshi Shimohata[3], Osamu Onodera[4], Christopher A. Ross[7,8,9], Motoya Katsuki[13], Hitoshi Takahashi[2], Masanobu Kano[6,§], Toshihiko Aosaki[5] and Shoji Tsuji[14,*]

[1]Department of Comparative and Experimental Medicine, [2]Department of Pathology, [3]Department of Neurology and [4]Department of Molecular Neuroscience, Brain Research Institute, Niigata University, Niigata 951-8585, Japan, [5]Neural Circuits Dynamics Research Group, Tokyo Metropolitan Institute of Gerontology, Itabashi-ku, Tokyo 173-0015, Japan, [6]Department of Cellular Neurophysiology, Graduate School of Medical Science, Kanazawa University, Kanazawa, Ishikawa 920-8640, Japan, [7]Department of Psychiatry, [8]Department of Neurology and [9]Department of Neuroscience, The Johns Hopkins University School of Medicine, Baltimore, MD 21287, USA, [10]Laboratory of Research Resources, National Institute for Longevity Sciences, Obu, Aichi 474-8522, Japan, [11]Department of Anesthesiology, School of Medicine, Juntendo University, Bunkyo-ku, Tokyo 113-8421, Japan, [12]Institute of Neuroscience, National Yang-Ming University, Li-Rum Street, Taiwan 11221, Taiwan, [13]National Institute for Basic Biology, Okazaki National Research Institutes, Okazaki, Aichi 444-8585, Japan and [14]Department of Neurology, Graduate School of Medicine, University of Tokyo, Bunkyo-ku, Tokyo 113-8655, Japan

Received August 1, 2008; Revised and Accepted November 25, 2008

We herein provide a thorough description of new transgenic mouse models for dentatorubral–pallidoluysian atrophy (DRPLA) harboring a single copy of the full-length human mutant *DRPLA* gene with 76 and 129 CAG repeats. The Q129 mouse line was unexpectedly obtained by *en masse* expansion based on the somatic instability of 76 CAG repeats *in vivo*. The mRNA expression levels of both Q76 and Q129 transgenes were each 80% of that of the endogenous mouse gene, whereas only the Q129 mice exhibited devastating progressive neurological phenotypes similar to those of juvenile-onset DRPLA patients. Electrophysiological studies of the Q129 mice demonstrated age-dependent and region-specific presynaptic dysfunction in the globus pallidus and cerebellum. Progressive shrinkage of distal dendrites of Purkinje cells and decreased currents through α-amino-3-hydroxy-5-methyl-4-isoxazolepropionic acid and γ-aminobutyrate type A receptors in CA1 neurons were also observed. Neuropathological studies of the Q129 mice revealed progressive brain atrophy, but no obvious neuronal loss, associated with massive neuronal intranuclear accumulation (NIA) of mutant proteins with expanded polyglutamine stretches starting on postnatal day 4, whereas NIA in the Q76 mice appeared later with regional specificity to the vulnerable regions of DRPLA. Expression profile analyses demonstrated age-dependent down-regulation of genes, including those relevant to synaptic

*To whom correspondence should be addressed. Tel: +81 358006542; Fax: +81 358006844; Email: tsuji@m.u-tokyo.ac.jp
†Present address: Department of Neuropharmacology, Graduate School of Medicine, Hokkaido University, Kita-ku, Sapporo 060-8638, Japan.
‡Present address: Academic Neurology Unit, The University of Sheffield Medical School, Beech Hill Road, Sheffield S10 2RX, UK.
¶Present address: Department of Psychiatry, McLean Hospital, Harvard Medical School, Belmont, MA 02478, USA.
§Present address: Department of Neurophysiology, Graduate School of Medicine, University of Tokyo, Bunkyo-ku, Tokyo 113-0033, Japan.

functions and CREB-dependent genes. These results suggest that neuronal dysfunction without neuronal death is the essential pathophysiologic process and that the age-dependent NIA is associated with nuclear dysfunction including transcriptional dysregulations. Thus, our Q129 mice should be highly valuable for investigating the mechanisms of disease pathogenesis and therapeutic interventions.

INTRODUCTION

Dentatorubral–pallidoluysian atrophy (DRPLA; MIM 125370) is a devastating, autosomal-dominant neurodegenerative disease characterized by progressive dementia, cerebellar ataxia, choreoathetosis, myoclonus and epilepsy in various combinations depending on the age at onset (1). As indicated by the name, autopsied brains show a selective neuronal loss associated with astrocytosis in the dentatorubral and pallidoluysian (DRPL) systems (2). In 1994, we and another group, focusing on genes containing CAG repeats (3), found that DRPLA is caused by an unstable expansion of CAG repeats coding for polyglutamine (polyQ) stretches in exon 5 of the *DRPLA* gene on chromosome 12p13.31 (4,5). To date, polyQ expansions have been identified as the pathogenic mutations in nine neurodegenerative diseases including Huntington's disease (HD), spinal and bulbar muscular atrophy, DRPLA and various forms of dominant spinocerebellar ataxias (SCAs) (6).

The discovery of neuronal intranuclear inclusions (NIIs) not only in brains of transgenic mice (7) but also in autopsied brains with polyQ diseases (8,9) provided new insight into neuronal nuclei as a potentially important site of pathogenic mechanisms. More importantly, we demonstrated that a diffuse accumulation of a mutant DRPLA protein (atrophin-1) in the neuronal nuclei of autopsied brains, rather than the formation of NIIs, is the predominant pathologic condition involving a wide range of central nervous system (CNS) regions far beyond the vulnerable DRPL systems (10). To further emphasize the involvement of nuclear dysfunction in polyQ diseases, we have demonstrated that expanded polyQ stretches bind to TATA-binding protein (TBP)-associated factors ($TAF_{II}130$) and cAMP response element-binding protein (CREB)-binding protein (CBP), which are components of transcriptional regulators (11,12). Taken together, these findings strongly suggest that essential pathogenetic processes occur in neuronal nuclei. The molecular mechanisms of neurodegeneration, however, remain to be elucidated.

To investigate these molecular mechanisms, studies on animal models precisely replicating all the processes in the human brain would be indispensable. For high-quality animal models, the expression of a full-length mutant gene under the control of its own promoter is preferable to those expressing truncated mutant proteins or under the control of potent heterologous promoters. To meet these requirements, we have generated transgenic mice harboring a single copy of the full-length human mutant *DRPLA* gene containing 76 CAG repeats (13). These Q76 mice did not exhibit obvious neurological phenotypes. During intensive breeding of Q76 mice, however, we unexpectedly found a mosaic mouse harboring largely expanded CAG repeats (Q129), in addition to the 76 repeats from progenitor mice, which bred transgenic offspring carrying 129 CAG repeats exhibiting distinct behavioral abnormalities. The Q129 mice showed severe neurological phenotypes with progressive brain atrophy and premature death. Some neuropathological findings of the Q129 mice at 14 weeks of age focusing on morphometric analysis have recently been reported, which demonstrate atrophy of the perikarya and dendrites, and a decrease in the number and size of the spines without any obvious neuronal loss (14). We herein report a thorough characterization of the phenotypes of Q129 mice, including electrophysiological abnormalities, neuropathological findings focusing on age-dependent neuronal intranuclear accumulation (NIA) of mutant DRPLA proteins and nuclear dysfunction assessed by expression profiling. As shown here, Q129 mice harboring a single copy of the full-length *DRPLA* gene have many advantages over the previous Q76 mice, and should serve as excellent models for exploring the molecular mechanisms of CAG repeat instability, disease pathogenesis and, furthermore, therapeutic intervention for polyQ diseases.

RESULTS

En masse expansion of CAG repeats occurred via somatic instability in a Q76 mouse

We previously established three transgenic lines, which were generated by the transfer of a cosmid genomic clone containing the full-length human mutant *DRPLA* gene with 78 CAG repeats (13). Although the mice showed intergenerational instabilities of CAG repeats similar to those observed in DRPLA patients, no obvious abnormal phenotypes were detected. To investigate intergenerational instabilities, we continued our extensive breeding of the Drm21 line carrying the 76 CAG repeats (Q76 mice). During the process, we unexpectedly noticed one male mouse (EF121) carrying both 76 and 129 CAG repeats among over 2000 hemizygous mice [Fig. 1A, Mosaic (Q129-76)]. After the birth of the EF121 mouse, the male parent of the EF121 mouse bred only Q76 or non-transgenic (non-TG) mice ($n = 66$ and 54, respectively). On the other hand, the highly expanded 129 CAG repeats, of which sequence was uninterrupted (unpublished data), were transmitted from the EF121 mouse to certain offspring exhibiting behavioral abnormalities (Q129 mice). These results suggest that the EF121 mouse is a mosaic with respect to the length of CAG repeats of the transgene and that the 129 CAG repeats were presumably generated by the *en masse* expansion of the 76 CAG repeats at the early embryonic stage.

Although the EF121 mosaic mouse was smaller than the Q76 mice and exhibited a slightly ataxic phenotype with age, the mouse was able to continue to breed and sired 528 mice by 122 weeks of age. The percentages of transgenic offspring of Q129, Q76 and non-TG mice bred from the EF121 mosaic mouse were 19% ($n = 98$), 32% ($n = 170$) and 49% ($n = 260$), respectively. Because one-half of the offspring were non-TG mice, the EF121 mosaic mouse was considered to be a hemizygote. Furthermore, the segregation ratios of 19

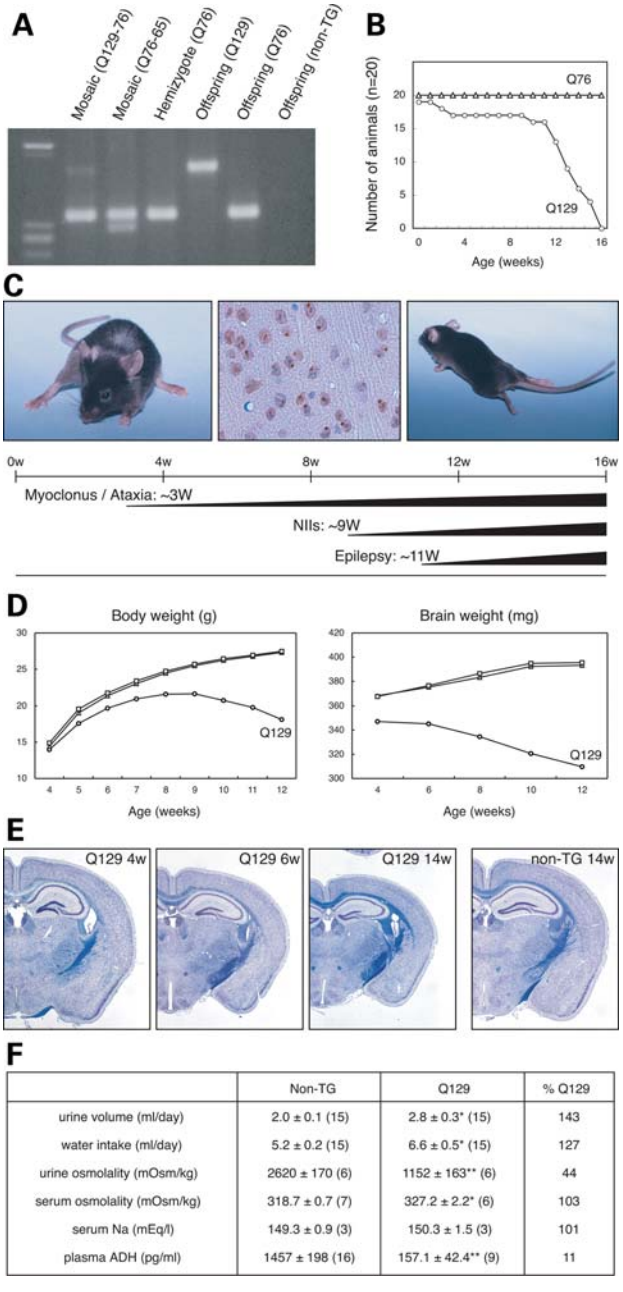

F

	Non-TG	Q129	% Q129
urine volume (ml/day)	2.0 ± 0.1 (15)	2.8 ± 0.3* (15)	143
water intake (ml/day)	5.2 ± 0.2 (15)	6.6 ± 0.5* (15)	127
urine osmolality (mOsm/kg)	2620 ± 170 (6)	1152 ± 163** (6)	44
serum osmolality (mOsm/kg)	318.7 ± 0.7 (7)	327.2 ± 2.2* (6)	103
serum Na (mEq/l)	149.3 ± 0.9 (3)	150.3 ± 1.5 (3)	101
plasma ADH (pg/ml)	1457 ± 198 (16)	157.1 ± 42.4** (9)	11

Figure 1. Generation of Q129 transgenic mice and disease phenotypes. (**A**) PCR analysis of tail DNA revealed two hemizygous mosaic mice (Q129-76 and Q76-65), a hemizygous mouse (Q76) and the offspring of the Q129-76 mosaic mouse showing three genotypes (Q129, Q76 and non-TG). The lane for the Q129-76 mosaic mouse showed a faint extra band of a much larger size than the band corresponding to 76 CAG repeats. The large changes in the size of CAG repeats resulted in not only expansion (Q129-76), but also contraction (Q76-65). (**B**) Kaplan–Meier survival curves of Q76 (triangles) and Q129 (circles) mice, showing premature death of Q129 mice ($n = 20$). (**C**) Representative photographs of the Q129 mice at 12 weeks (W), showing ataxic phenotype (left panel), ubiquitinated NIIs (middle panel) and epileptic seizure (right panel). (**D**) Changes in body and brain weights of the Q129 (circles), Q76 (triangles) and non-TG (rectangles) mice. Each value and number of replicates is shown in Supplementary Material, Tables S1 and S2. (**E**) Cross-sections of brains of the Q129 mice (4W, 6W and 14W) and non-TG littermate (14W) (Klüver–Barrera staining), showing progressive reduction in brain size of Q129 mice. (**F**) Results of laboratory tests indicate central diabetes insipidus. Each value indicates mean ± S.E.M. Unpaired *t*-test, $^{*}P < 0.05$, $^{**}P < 0.01$. Numbers of replicates are shown in parentheses.

and 32% suggested that the *en masse* expansion of the CAG repeats had occurred either at the two-cell or four-cell stage. The Q129 mice were established by *in vitro* fertilization because of their decreased fertility. The fertilizing ability of spermatozoa from the Q129 mice was comparable to that of the wild-type mice, suggesting that the reduced fertility is due to behavioral abnormalities.

Phenotypes of Q129 mice are similar to those of juvenile-onset DRPLA patients

The onset of symptoms was as early as 3 weeks of age, at which the Q129 mice began to show myoclonic movements and mild ataxia (Fig. 1C). When held by the tail, the myoclonic movements were more evident with limbs outstretched. The clasping of hindlimbs was hardly observed. The myoclonic movements and ataxia rapidly progressed, and epilepsy was observed at around 11 weeks. Initially, epilepsy was induced by tactile stimuli and at the later stage, it occurred spontaneously, even in their home cages. The rapid progression of the disease phenotype was followed by premature death, and all the Q129 mice died by 16 weeks (Fig. 1B and C; Supplementary Material, Videos S1 and S2, ataxia and epilepsy, respectively). The severe neurological phenotypes observed in the Q129 mice, namely myoclonus and epilepsy, were quite similar to those observed in juvenile-onset DRPLA patients with onset before the age of 20 (1,15). These phenotypes are in striking contrast to those of the Q76 mice that do not show any obvious neurological phenotypes.

The brain weight was less than that of the Q76 or non-TG mice at 4 weeks of age, even at a time when body weight did not change. Along with the disease progression, the brain weight of the Q129 mice further decreased after 6 weeks of age prior to the decrease in body weight (Fig. 1D; Supplementary Material, Tables S1 and S2). The examination of brain cross-sections further demonstrated the age-dependent decrease in the brain size of the Q129 mice at 4, 6 and 14 weeks of age (Fig. 1E). In addition, the Q129 mice became polyuric around 5 weeks of age, a phenomenon that was not observed in the Q76 mice. Detailed analyses of water balance were conducted at 8 weeks of age. The Q129 mice showed increased urine volume, water intake and serum osmolality, and reduced urine osmolality (Fig. 1F). Furthermore, we found a drastic reduction in the plasma vasopressin (anti-diuretic hormone) level, confirming that the Q129 mice suffered from central diabetes insipidus.

Dysfunction of pallidal and cerebellar neurons correlates with disease manifestations and progression

We first conducted electrophysiological studies of the globus pallidus (GP) and cerebellum, because these structures are highly associated with neuropathological changes in DRPLA. Using the Q129 and non-TG mice at 4–5 weeks of age, we performed whole-cell recordings from pallidal neurons. Excitatory (EPSCs) and inhibitory postsynaptic currents (IPSCs) were evoked by activating the sub-thalamopallidal and striatopallidal pathways, respectively. We did not detect any significant differences in input–output (I–O) relationships (Fig. 2Aa). In addition, current–voltage (*I–V*) relationships and the

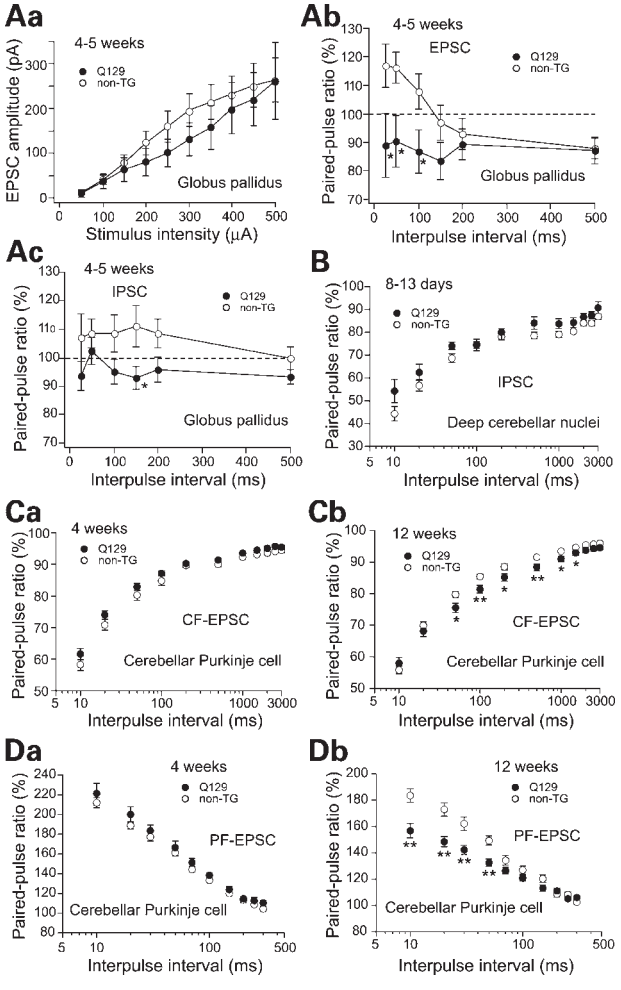

Figure 2. Age-dependent abnormalities of synaptic transmission in GP and cerebellum. Pallidal and cerebellar slices were obtained from the Q129 mice (filled circles) and non-TG mice (open circles) at various ages as indicated in each figure. (**Aa**–**Ac**) Whole-cell recordings from pallidal neurons of the Q129 and non-TG mice at 4–5 weeks of age. I–O relationship for EPSC (**Aa**), PPRs for EPSC (**Ab**) and IPSC (**Ac**) in GP. EPSCs and IPSCs were evoked by stimulating the sub-thalamopallidal and striatopallidal pathways, respectively, at 0.1 Hz with a bipolar tungsten electrode (100–500 μs, 100–800 μA). IPSCs were recorded at a holding potential of −10 mV in the presence of CNQX and D-AP5. EPSCs of the Q129 mice ($n = 14$) tended to be smaller than those of the non-TG mice ($n = 21$), which showed no statistically significant difference (**Aa**). PPRs for EPSC (**Ab**) and IPSC (**Ac**) in the Q129 mice ($n = 12$ and 11, respectively) decreased as compared with those of the non-TG mice ($n = 22$ and 15, respectively), resulting in the conversion of PPF to PPD in the Q129 mice at 4–5 weeks of age. (**B**) PPR for IPSC in FN on postnatal days 8–13. IPSCs were evoked by stimulating bundles of putative PC axons. There was no significant difference between the Q129 mice ($n = 12$) and the non-TG mice ($n = 30$). (**Ca**–**Db**) Age-dependent changes in PPRs for CF-EPSCs and PF-EPSCs. CF-EPSCs were recorded from PCs at 4 (**Ca**) and 12 weeks (**Cb**) of age in the Q129 ($n =$ 19 and 27, respectively) and non-TG mice ($n = 20$ and 30, respectively). PF-EPSCs were recorded from PCs at 4 (**Da**) and 12 weeks (**Db**) of age in the Q129 ($n = 14$ and 27, respectively) and non-TG mice ($n = 22$ and 28, respectively). For focal stimulation in the cerebellar slices, we used a bipolar tungsten electrode (for PC axons) and glass pipettes (5–10-μm tip diameter) filled with standard saline (for CFs and PFs), and applied square pulses (duration, 100 μs; amplitude, 0–90 V) at 0.5 Hz. Bundles of putative PC axons were stimulated in the white matter 100–200 μm away from the FN. CFs were stimulated in the granule cell layer 50–100 μm away from the PC soma. PFs were stimulated in the middle of the molecular layer. Each value indicates mean ± S.E.M. Unpaired *t*-test, $^{*}P < 0.05$, $^{**}P < 0.01$. Note that the abscissas of **B**–**Db** are shown in the logarithmic scale.

amplitudes of both *N*-methyl-D-aspartate (NMDA) and α-amino-3-hydroxy-5-methyl-4-isoxazolepropionic acid (AMPA) components of EPSCs were not significantly different (unpublished data). In contrast, the paired pulse facilitation (PPF) of EPSCs and IPSCs was clearly converted to paired pulse depression (PPD) in the Q129 mice (Fig. 2Ab and Ac), suggesting presynaptic dysfunction in GP of the Q129 mice at 4–5 weeks of age.

For electrophysiological studies of the cerebellum, we conducted whole-cell recordings from medium to large neurons in the fastigial nucleus (FN) obtained from young asymptomatic mice aged 8–13 days. IPSCs evoked by stimulating putative Purkinje cell (PC) axons displayed PPD in both non-TG and Q129 mice (Fig. 2B). There was no significant difference in the extent of PPD. Thus, on postnatal days 8–13 before the manifestation of ataxia, transmission from PCs to neurons in FN (one of the deep cerebellar nuclei) in the Q129 mice was apparently normal. Further studies of neurons in the GP and FN at later stages could not be performed because of the limited time window suitable for such electrophysiological analyses.

To investigate age-dependent changes in the cerebellum, we next compared the electrophysiological properties of PCs at 4 and 12 weeks of age. The passive membrane properties of PCs were calculated by recording membrane currents in response to hyperpolarizing voltage steps, as described previously (16). We found that the C2 of the Q129 mice, representing the lumped membrane capacitance of the PC's dendritic tree, was significantly smaller than that of the non-TG mice at 12 weeks of age ($P < 0.01$), whereas no significant changes were observed at 4 weeks of age (Table 1). In addition, R3 of the Q129 mice, representing the lumped resistance of the PC's dendritic tree, tended to be greater than that of the non-TG mice at 12 weeks of age. These results suggest that the PC's dendritic trees of the Q129 mice markedly shrank in a time-dependent manner.

We then examined whether excitatory synaptic transmission to PCs is altered in the Q129 mice. We recorded EPSCs from PCs by stimulating climbing fibers (CFs: axons of inferior olivary neurons) or parallel fibers (PFs: axons of granule cells). We first confirmed that the number of CFs innervating a PC was not significantly different between the non-TG and Q129 mice at 4 or 12 weeks of age (unpublished data). As for the kinetics of CF-EPSCs, the rise time or amplitude was not significantly altered in the Q129 mice except for a slight decrease in the decay time constant in the Q129 mice at 4 and 12 weeks of age (Table 1). At 4 weeks of age, there was no significant difference in the extent of PPD of CF-EPSC or PPF of PF-EPSC (Fig. 2Ca and Da). At 12 weeks of age, however, paired pulse ratios (PPRs) for CF-EPSC and PF-EPSC in the Q129 mice were significantly smaller than those in the non-TG mice at interpulse intervals of 50–1500 ms and those at intervals of shorter than 50 ms, respectively (Fig. 2Cb and Db).

Dysfunction of synaptic transmission in hippocampal CA1 pyramidal cells

Although the hippocampus is not a severely affected region in DRPLA, NIA of mutant DRPLA proteins was observed in juvenile-onset DRPLA patients (10), and also confirmed in

Table 1. Electrophysiological parameters of PCs

	Non-TG	Q129
Postnatal 4 weeks		
Passive membrane properties[a]	$n = 6$	$n = 11$
C1 (pF)	60.4 ± 8.8	69.8 ± 10.0
C2 (pF)	617.3 ± 58.8	571.2 ± 46.8
R1 (MΩ)	14.8 ± 3.4	13.2 ± 1.2
R2 (MΩ)	21.3 ± 5.1	19.4 ± 2.0
R3 (MΩ)	308.1 ± 68.2	211.0 ± 29.9
CF-EPSC	$n = 15$	$n = 18$
10–90% rise time (ms)	0.4 ± 0.01	0.4 ± 0.01
Decay time constant (ms)[b]	7.7 ± 0.3**	6.6 ± 0.3**
Amplitude at −10 mV (pA)	1114.1 ± 111.4	1126.2 ± 139.9
Amplitude at +50 mV (pA)	768.1 ± 179.6	812.2 ± 241.8
Postnatal 12 weeks		
Passive membrane properties[a]	$n = 14$	$n = 19$
C1 (pF)	95.5 ± 13.4	80.8 ± 11.1
C2 (pF)	629.9 ± 63.5**	332.6 ± 18.9**
R1 (MΩ)	11.1 ± 0.6	11.4 ± 1.1
R2 (MΩ)	15.8 ± 3.8	16.7 ± 1.7
R3 (MΩ)	241.2 ± 47.4	405.3 ± 76.5
CF-EPSC	n=23	$n = 26$
10–90% rise time (ms)	0.4 ± 0.03	0.4 ± 0.01
Decay time constant (ms)[b]	6.9 ± 0.3**	5.9 ± 0.3**
Amplitude at −10 mV (pA)	1150.9 ± 98.8	1312.0 ± 140.4
Amplitude at +50 mV (pA)	1085.2 ± 182.9	1771.3 ± 297.7

[a] Parameters for passive membrane properties are calculated according to the model described by Llano *et al*. (16), which distinguishes two regions of PCs: region 1, representing the soma and the main proximal dendrites, and region 2, representing the dendritic tree. C1 and C2 represent the lumped membrane capacitance of regions 1 and 2, respectively. R1 represents the pipette access resistance. Region 2 is linked to region 1 by resistor R2, representing the lumped resistance between the main proximal dendrite and each membrane region of distal dendrites. R3 represents the lumped resistance of the dendritic tree of PCs. C1, C2, R1 and R2 are calculated from the initial capacitive currents in response to hyperpolarizing voltage steps (500-ms duration) from −70 to −80 mV. R3 is measured from the steady-state currents in response to hyperpolarizing voltage steps (500-ms duration) from −80 to −85 mV.
[b] Decay time constants for CF-EPSC are measured by fitting EPSC decay with a single exponential. The holding potential was −80 mV.
All data are expressed as mean ± S.E.M.
**$P < 0.01$ (*t*-test).

Q76 (Table 2) and Q129 mice (14), indicating that the hippocampus may well be involved in the pathological processes of DRPLA. To evaluate the electrophysiological properties of hippocampal CA1 pyramidal cells, we first analyzed basal synaptic transmission by applying electrical stimuli of increasing intensity to the Schaffer collateral/commissural pathway using Q129 and non-TG mice at 12–15 weeks of age. The extracellular recordings showed that the field excitatory postsynaptic potential (fEPSP) slopes of the Q129 mice were significantly smaller than those of the non-TG mice at 12–15 weeks of age (Fig. 3A). A significantly enhanced PPF was also observed in the Q129 mice (Fig. 3B at 100 ms, $P = 0.024$; at 150 ms, $P = 0.002$), suggesting presynaptic dysfunction.

In the whole-cell recordings from CA1 neurons, the ratio of NMDA/AMPA currents in the Q129 mice was significantly larger than that in the non-TG mice, despite the observation that *I–V* relationships of AMPA, NMDA and γ-aminobutyrate type A ($GABA_A$) currents were unchanged (unpublished data). To further investigate the mechanisms underlying the increased ratio of NMDA/AMPA currents, we compared responses to the agonists of AMPA, NMDA and $GABA_A$ receptors. AMPA-induced inward currents were significantly smaller in the Q129 mice than in the non-TG mice across the five concentrations tested (Fig. 3Ea), whereas there were no significant changes in NMDA-induced inward currents (Fig. 3Eb). Similar to AMPA currents, $GABA_A$-induced outward currents were significantly smaller in the Q129 mice than in the non-TG mice at elevated muscimol concentrations (Fig. 3Ec).

We next analyzed the long-term potentiation (LTP) of fEPSPs in the hippocampal CA1 region. LTP induced by one train of tetanic stimulation lasted for more than 4 h in the non-TG mice, whereas it subsided within 2 h in the Q129 mice (Fig. 3C). The average fEPSP slope within a time window of 120–180 min after tetanus in the Q129 mice was 98.7 ± 9.3%, which was significantly lower than that in the non-TG mice (132.8 ± 4.5%, $P = 0.004$). In contrast, four trains of tetanic stimulation induced late-phase LTP in both genotypes to the same extent (Fig. 3D).

Age- and expanded-polyQ-length-dependent NIA of mutant DRPLA proteins

In accordance with our previous findings in the Q129 mice at 14 weeks of age (14), an age-dependent decrease in the brain size of the Q129 mice was evident (Fig. 1E), but neuronal loss or astrocytosis was not evident despite the progressive brain atrophy (Fig. 4). In hematoxylin- and eosin-stained preparations, small eosinophilic intranuclear inclusions were detectable in some neurons of restricted CNS regions of the Q129 mice after 12 weeks of age (unpublished data). In immunohistochemical analysis using anti-ubiquitin antibodies, they were easily detected after 9 weeks of age as ubiquitinated NIIs in multiple CNS regions such as the cerebral cortex, GP, subthalamic nucleus (luysian body), brainstem tegmentum and deep cerebellar nuclei (Fig. 1C). It should be noted, however, that NIIs were formed much later than the onset of neurological phenotypes, suggesting that the disease phenotypes do not arise from the formation of NIIs. In contrast to the Q129 mice, we did not detect any evidence of NIIs in the brain of Q76 mice even at 122 weeks of age (unpublished data).

To find age-dependent changes focusing on the regional distribution of NIA, we performed immunohistochemical analyses of the Q76 and Q129 mice at various weeks of age using highly diluted 1C2 (1:16 000). At this dilution, no background immunoreactivities were detected in the brain of the non-TG mice, confirming that 1C2 immunoreactivity is specific to the expanded polyQ stretches of mutant proteins (Fig. 4A, right panels) (10). In contrast to the non-TG mice, 1C2 immunoreactivity was clearly evident as a diffuse nuclear labeling of neurons in the 4-week-old brain of the Q129 mice (Fig. 4A, middle panels). The nuclear labeling, namely NIA, was strong and extended to most of the CNS regions including the brainstem, spinal cord and the regions evaluated for the above-mentioned electrophysiological properties. It should be noted that NIA, which was observed at 4 weeks of age in the Q129 mice, occurred much earlier than the appearance of NIIs after approximately 9 weeks of age. To determine when NIA becomes apparent, we further

Table 2. Distribution of NIA of expanded polyQ stretches in Q76 mice

Region	Gestational age			Region	Gestational age		
	4W	8W	14W		4W	8W	14W
Cerebral cortex				Thalamic nuclei			
II	−	+	++	Centrolateral	−	−	++
III	−	+	+++	Ventroposterior	−	−	+
IV	+	+++	+++	Reticular	−	−	++
V	−	+	+	Subthalamic nucleus	+	++	+++
VI	−	++	+++	Hypothalamic nuclei	−	+	++
Piriform cortex	−	+	++	Substantia nigra			
Caudate-putamen	−	+	++	Pars compacta	−	++	+++
Globus pallidus	+	++	+++	Pars reticulata	−	+	++
Hippocampus				Superior colliculus	−	+	+++
CA1	−	−	+	Periaqueductal gray	−	+	++
CA2	−	−	+	Deep mesencephalic nucleus	−	+	+++
CA3	−	−	+	Red nucleus	+	++	+++
Dentate gyrus				Pontine nuclei	−	+	+++
Granule cell layer	−	−	+	Pontine reticular nucleus	+	++	+++
Polymorphic cell layer	−	−	+	Vestibular nucleus	−	++	+++
Amygdaloid nuclei	+	+	++	Facial nucleus	−	−	−
Lateral habenular nucleus	−	+	+++	Inferior olive	−	−	−
Medial habenular nucleus	−	−	−	Gigantocellular reticular field	+	++	+++
Thalamic nuclei				Purkinje cell	−	−	−
Mediodorsal	−	−	+	Granule cell	−	+	++
Centromedial	−	−	++	Cerebellar nuclei	+	++	+++

At 4 weeks of age, nuclear labeling was detected not only in the DRPL systems, but also in some brain regions including the cerebral cortex and brainstem nuclei. Thereafter, the number and intensity of labeled neurons increased gradually throughout the brain with a specific distribution pattern. Percentage of labeled neurons: −, none; +, <30%; ++, 30–70%; +++, >70%.

analyzed the Q129 mice on embryonic and postnatal days. NIA was not observed in the brain of Q129 mice on postnatal day 1 (P1), but became detectable on P4, confirming age-dependent NIA of mutant DRPLA proteins (Fig. 4B).

Interestingly, NIA was also observed in the Q76 mouse brain despite the Q76 mice not showing any obvious neurological phenotypes. In contrast to the Q129 mice, the intensity of NIA was weak in the brains of Q76 mice, but increased with age (Fig. 4A, left panels). The regional distribution of NIA in the Q76 mice was analyzed semiquantitatively (Table 2). NIA was first detectable at 4 weeks of age in limited CNS regions, such as the cerebellar nuclei, red nucleus, GP, subthalamic nucleus and a few other regions including the cerebral cortex of the Q76 mice. It is noteworthy that the former four regions are the sites known to be the most vulnerable to DRPLA (1,2). Furthermore, the distribution of NIA in the brains of Q76 mice at 14 weeks of age became similar to that of NIIs in the brains of Q129 mice.

Since 1C2 immunoreactivity varies depending on the length of polyQ stretches, immunohistochemical analyses with 1C2 may produce some bias in terms of accumulation of mutant DRPLA proteins with different lengths of expanded polyQ stretches. We further conducted immunohistochemical analyses using APG840 raised against residues 425–439 of the DRPLA protein (10) that correspond to the upstream region of the polyQ stretches. In contrast to 1C2, APG840 recognized not only human mutant DRPLA proteins, but also endogenous mouse wild-type DRPLA proteins (Fig. 4C). Although background nuclear staining was observed in the non-TG mice as APG840 recognized mouse DRPLA protein, strong nuclear staining was observed in the Q129 mice at as early as 4 weeks of age. In the Q76 mice, mild but increased staining was observed at 14 weeks compared with that at 4 weeks. These findings further confirm polyQ-length-dependent and age-dependent intranuclear accumulation of mutant DRPLA proteins.

Massive accumulation of mutant DRPLA proteins in Q129 mouse brain

First, we performed quantitative analyses of the mRNA expression levels of the human *DRPLA* transgene and endogenous mouse *DRPLA* gene in the brains of the Q76 and Q129 mice at 8 weeks of age by competitive reverse transcription–polymerase chain reaction (RT–PCR) (Fig. 5A). After confirming the validity of the quantitative analysis by PCR, the mRNA expression levels of the transgenes of the Q129 and Q76 mice were determined to be ∼80% of the mouse endogenous level.

Western blot analysis was performed using three antibodies: C580 (17; a polyclonal antibody against the carboxyl terminus of the DRPLA protein), AP142 (18; a polyclonal antibody against residues 425–439) and 1C2 (specifically recognizes expanded polyQ stretches). In the total homogenates of the mouse brain, two bands corresponding to the full-length mouse endogenous DRPLA protein (200 kDa) and transgene-derived DRPLA proteins (210 and 220 kDa in Q76 and Q129, respectively) were detected using C580, whereas only the lower band corresponding to the full-length mouse DRPLA protein was observed for the non-TG mice (Fig. 5B). In addition to the 200-kDa band, a 100-kDa band was detected in human autopsied control brain, consistent with previous observations on human DRPLA brains employing C580 (17). The intensities of the bands of the full-length DRPLA proteins of Q129 were much weaker than those corresponding

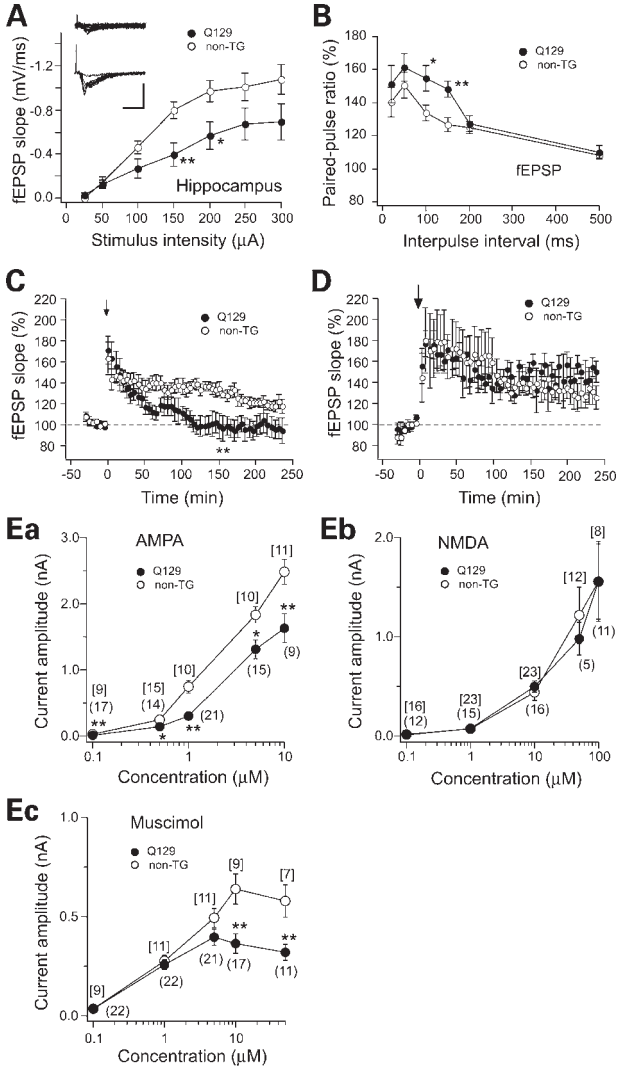

Figure 3. Abnormalities of synaptic transmission and plasticity in hippocampus. Hippocampal slices were obtained from the Q129 mice (filled circles) and the non-TG mice (open circles) at 12–15 weeks of age. (**A**) The I–O relationship showed a significant attenuation of the responsiveness of CA1 pyramidal cells in the Q129 mice ($n = 12$) as compared with that in the non-TG mice ($n = 13$). The slopes of fEPSPs evoked by stimulating the Schaffer collateral/commissural pathway are plotted against stimulus intensity. Inset: examples of fEPSPs of the Q129 (upper) mouse and the non-TG (lower) mouse. Scale bars: 2 mV/10 ms. (**B**) The PPR for the fEPSP slope of CA1 hippocampal cells in the Q129 mice ($n = 12$) was enhanced as compared with that in the non-TG mice ($n = 13$) at 13–15 weeks of age. (**C**) LTP induced by one train of tetanus (a small arrow) subsided within 120 min in the Q129 mice ($n = 10$), whereas LTP in the non-TG mice ($n = 10$) lasted much longer. (**D**) Late-phase LTP induced by four trains of tetanus (a large arrow) was not significantly different between the Q129 mice ($n = 5$) and the non-TG mice ($n = 5$). Data in **C** and **D** are normalized for each slice with respect to the average slope recorded during the baseline. (**Ea**–**Ec**) Pharmacological evidence for functional down-regulation of AMPA and $GABA_A$ receptors in hippocampus of Q129 mice at 12–15 weeks of age. AMPA-induced inward current (**Ea**) was recorded at a holding potential of −60 mV in the presence of 0.1 mM cyclothiazide, which prevents the rapid desensitization of AMPA receptors and 0.5 μM TTX. NMDA-induced inward current (**Eb**) was recorded at a holding potential of −40 mV in the presence of 20 μM glycine and 0.5 μM TTX in Mg^{2+}-free ACSF. Muscimol-induced outward current (**Ec**) was recorded at a holding potential of 0 mV. Drug exposure time was 1 min throughout the experiments. The flow rate was 2–3 ml/min. Each value indicates mean ± S.E.M. Unpaired *t*-test, $^{*}P < 0.05$, $^{**}P < 0.01$.

to the mouse endogenous DRPLA proteins or those of Q76, which may reflect the highly aggregatable nature of mutant DRPLA proteins with highly expanded polyQ stretches that may be resistant to extraction or solubilization procedures. Although the reason why the intensities of full-length mutant proteins decreased in the Q129 mice was unclear, a similar observation was described for *SCA1*$^{154Q/2Q}$ mice (19). The intensities of the bands detected by C580 were similar throughout the time course of 4, 8 and 12 weeks of age.

To further analyze the proteins accumulating in the nucleus, we prepared nuclear fractions employing the sucrose gradient centrifugation procedure as previously described (20) from the brains of Q129, Q76 and non-TG littermates at 12 weeks of age, and performed western blot analysis using AP142 that recognizes the segment upstream of polyQ stretches. A massive amount of smear migrating between the stacking gel and the band corresponding to the full-length mutant protein was observed for the Q129 mice, in addition to human full-length and truncated bands as well as the mouse endogenous band (Fig. 5C). The truncated proteins were also recognized by 1C2 (unpublished data) and thus specific for mutant DRPLA proteins as described previously (20). The smear was far more intense for the Q129 mice than for the Q76 mice, confirming the polyQ-length-dependent nuclear accumulation of the mutant proteins with expanded polyQ stretches. The smearing pattern was also observed in AT-FL-65Q-150 mice (Fig. 5C; lane 1) as previously described. AT-FL-65Q-150 mice are transgenic mice carrying full-length DRPLA cDNA under the control of the prion promoter and expressing higher levels of the transgene than the Q129 mice (20). Although the intensities of the truncated bands and the smears were considerably different between Q129 and AT-FL-65Q-150, this may reflect the higher expression levels of mutant DRPLA proteins in AT-FL-65Q-150 and regional differences in expression depending on the promoter driving the transgenes (Q129: own promoter of *DRPLA* gene; ATFL-65Q: prion promoter). The difference in the western blotting patterns detected by AP142 and C580 raises many possibilities, including that a fraction of accumulated mutant DRPLA proteins in the nucleus are truncated at the carboxy terminus. This possibility should be thoroughly investigated employing sensitive procedures including additional antibodies.

Transcriptional down-regulation becomes prominent in an age-dependent manner

As described above, the most fundamental pathological change was the age- and expanded-polyQ-length-dependent NIA of mutant proteins without any obvious neuronal loss, raising the possibility that such an NIA of mutant proteins leads to neuronal dysfunction including synaptic transmissions through transcriptional dysregulations. Thus, we analyzed expression profiles (∼11 000 genes) in the brains of the Q129 and non-TG littermates at 4 and 12 weeks of age using GeneChip Mu11K oligonucleotide microarrays (Affymetrix, Santa Clara, CA). To determine how gene expressions are affected as a function of disease duration, we selected dysregulated genes at each age using one-way analysis of variance (ANOVA) with error-weighting. On the basis of our criteria described in Materials and Methods, we detected 54 and 92

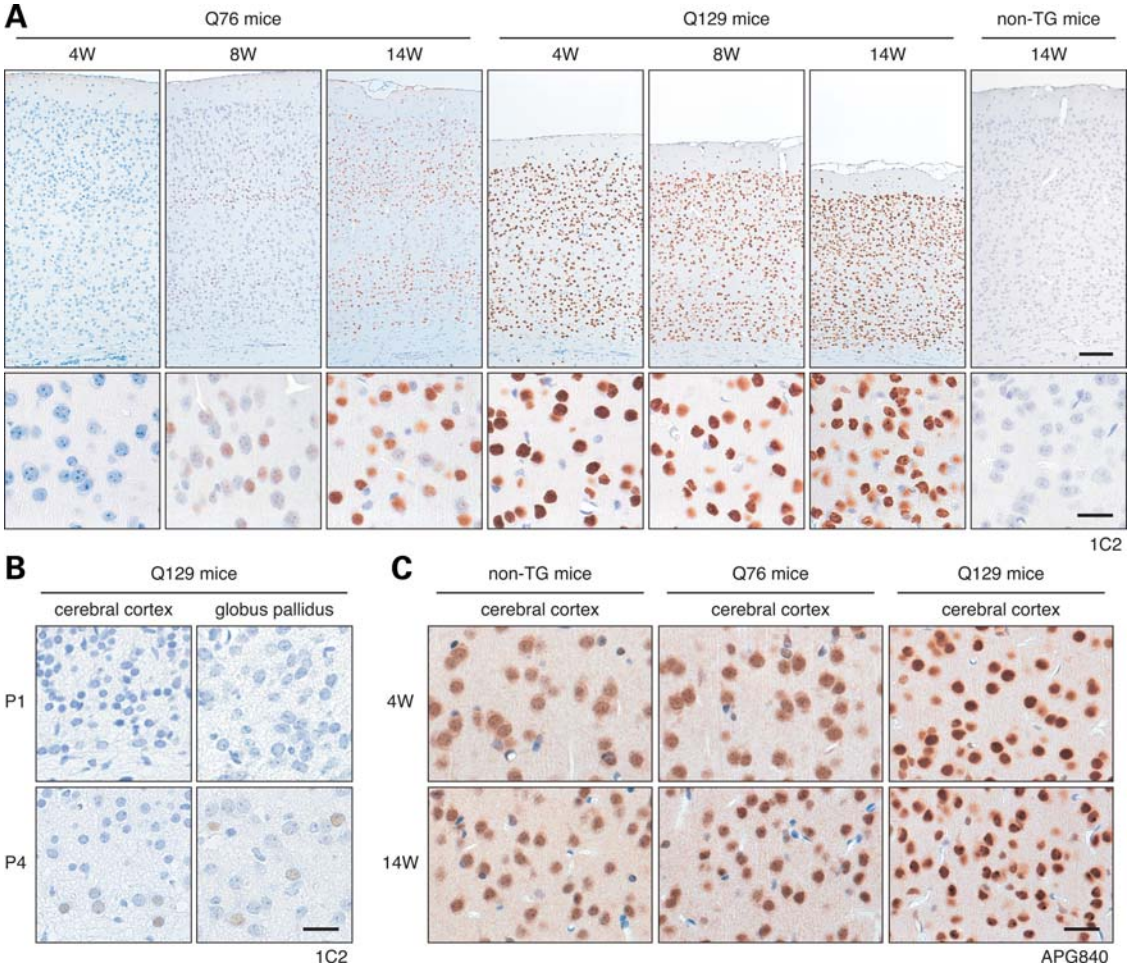

Figure 4. Age- and expanded-polyQ-length-dependent changes in NIA of mutant DRPLA proteins. (**A**) Immunohistochemical analysis of cerebral cortices of the Q76, Q129 and non-TG mice was performed using 1C2. The upper panels show the entire cerebral cortices and the lower panels show cortical layer III. In the Q129 mice (middle panels), the decrease in cortical size was already evident at 4 weeks of age and the cerebral cortex progressively atrophied with age. Neuronal nuclei in all the cortical layers showed intense labeling of expanded polyQ stretches and became gradually packed with age. Age-dependent nuclear atrophy and deformity were also observed (lower panels). There was no obvious neuronal loss in the Q129 mouse brain. In the Q76 mice (left panels), there was no obvious decrease in cortical size. In the lower panels, a gradual increase in the number of neuronal nuclei labeled by 1C2 was observed. Such nuclear labeling became evident particularly in the cortical layers IV and VI. Scale bar = 100 μm for upper panels and 20 μm for lower panels. (**B**) Immunohistochemical analysis of cerebral cortical layer VI and GP of the Q129 mice using 1C2 revealed faint NIA on P4, but not on P1. Scale bar=20 μm. (**C**) Immunohistochemical analysis of cerebral cortical layer III using APG840, an anti-DRPLA protein (atrophin-1) antibody, also revealed polyQ-length-dependent and age-dependent intranuclear accumulation of mutant DRPLA proteins. Scale bar = 20 μm.

down-regulated probe sets, as well as 38 and 20 up-regulated sets at 4 and 12 weeks of age, respectively. The number of down-regulated genes tended to increase with age. We next searched for genes showing age-dependent changes in the levels of expression determined by the two-way ANOVA. We found 46 down-regulated genes (corresponding to 48 probe sets on the microarrays) and 26 up-regulated genes. Interestingly, many of the down-regulated genes were categorized mainly into specific functional molecules, such as neuropeptides, transcriptional factors and signaling molecules (Fig. 6). Although all of the down-regulated genes showed further decreases in expression level with age, the degrees of decrease were different and a limited number of the genes, mainly categorized into neuropeptides, showed a marked decrease (fold change < -1.5) at 4 weeks of age. To determine the relevance of the down-regulated genes to CREB-dependent transcriptional dysregulation, we examined whether these down-regulated genes are candidates for CREB target genes (21,22). We found that 21 of the 46 (46%) down-regulated genes and 17 of the 28 (61%) strongly down-regulated genes (fold change < -1.5; shown in blue in Fig. 6) have cAMP response element (CRE) sites that are conserved between human and rodent orthologs. Among the down-regulated genes, we further confirmed decreased protein levels of arginine vasopressin (Fig. 1F) and kalirin (see Supplementary Material, Fig. S1).

DISCUSSION

Q129 mice as a model to understand the mechanisms of *en masse* expansion or contraction of CAG repeats

We established the Q129 DRPLA transgenic mice by utilizing a unique phenomenon, *en masse* expansion of CAG repeats.

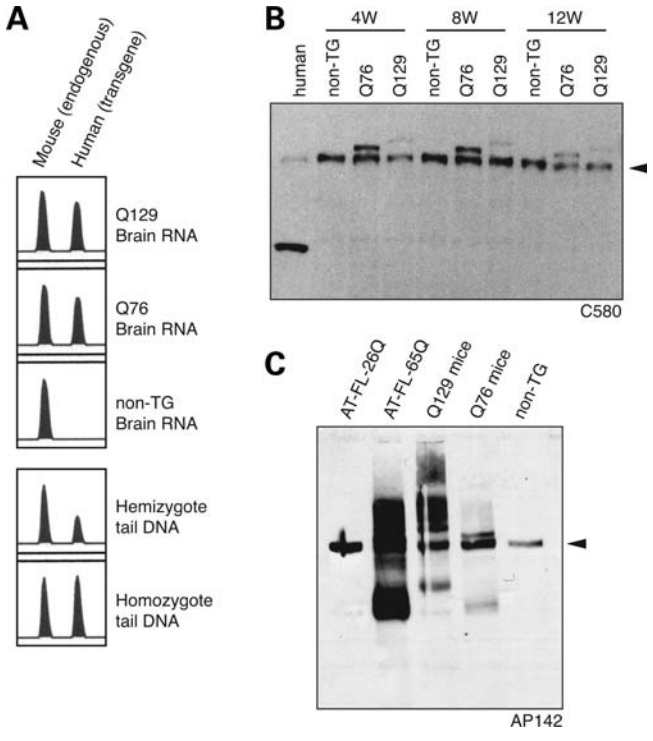

Figure 5. Quantification of mutant DRPLA mRNA levels and western blot analysis of DRPLA proteins in Q129 mouse brains. (**A**) The expression levels of DRPLA mRNAs derived from the transgene and mouse endogenous *DRPLA* gene were quantified by competitive RT–PCR. Considering that the length of the homo-serine stretch in the human *DRPLA* gene is 9 bp longer than that in the mouse *DRPLA* gene, we amplified a segment of DRPLA genomic DNA or cDNAs using flanking primers that completely match both the human and mouse genomic sequences. The validity of the quantitative analysis was confirmed by gene dosage analysis of human mutant transgenes when compared with endogenous mouse *DRPLA* genes. The expression levels of human *DRPLA* gene-derived mRNAs of Q129 and Q76 were determined for each to be 80% of the endogenous mouse DRPLA mRNA level. (**B**) Western blot analysis of total brain homogenates employing C580 revealed two bands corresponding to mouse endogenous (arrowheads) and transgene derived DRPLA proteins in the Q76 or Q129 mice. The lane for human control brain carrying 13 and 9 CAG repeats (lane 1) showed a weak band corresponding to the full-length human DRPLA protein. The intensities of the full-length protein in autopsied brains have been shown to be variable, possibly due to the intrinsic instability of the DRPLA protein, and the identity of the 100-kDa band detected by C580 remains unknown as previously described (17). (**C**) Western blot analysis of nuclear fractions using AP142 showed smears migrating between the stacking gel and the full-length bands. The smaller bands, possibly truncated, with polyQ-length-dependent mobility shifts were observed in Q129 and Q76. As a comparison, other DRPLA transgenic mouse models (20; AT-FL-26Q-84 and AT-FL-65Q-150 at 7.5 months of age) were also analyzed. In the lane for AT-FL-65Q mice, a massive amount of smears as well as truncated proteins with a faster mobility than those in the lane for Q129 mice were observed.

This is the first report of a polyQ model generated by *en masse* expansion. We previously showed age-dependent changes in expanded CAG repeats in somatic tissues as well as intergenerational instabilities of expanded CAG repeats (13). The mechanism of instability has been assumed to be cumulative accumulation of short repeat changes with age, typically one-repeat additions or subtractions. In contrast, *en masse* expansion (Fig. 1A, lane 1) or contraction (Fig. 1A, lane 2) is quite different in terms of the frequency and length of repeat changes. The large intergenerational increase in the CAG repeats to expanded alleles from the intermediate alleles has been observed in a small number of HD or SCA7 patients, and is called the *de novo* expansion (23–25). This phenomenon may be similar to the *en masse* expansion observed in this study. Based on these observations, there seem to be two discrete mechanisms of CAG repeat instability: cumulative accumulation of short repeat changes with age and *en masse* changes occurring spontaneously, but infrequently. Because the mosaic mice were hemizygous, inter-allelic recombination mechanisms are unlikely to be involved. We previously reported a patient with *en masse* expansion of impure CAG repeats in the TBP gene. In this case, inter-allelic recombination events were excluded on the basis of haplotype analysis (26). These intriguing observations suggest that simple intra-allelic rearrangements are involved in the CAG repeat instabilities associated with *en masse* expansions or contractions, which have also been suggested to be involved in somatic instability of minisatellites (27). Taking advantage of the instability of the 129 CAG repeats, we have recently obtained transgenic models carrying 113 or 96 CAG repeats with moderately severe neurological phenotypes (unpublished observation). Thus, transgenic models carrying single copy genes within a full-length genomic context may serve to produce those with variable lengths of expanded CAG repeats.

Q129 mice as an excellent model to understand disease pathogenesis of DRPLA

The Q129 and Q76 mice should be highly valuable for investigating expanded-polyQ-length-dependent effects, because the only difference between the Q129 and Q76 mice is the length of expanded CAG repeats within an identical integration site. The severe neurological phenotypes of the Q129 mice are quite similar to those observed in juvenile-onset DRPLA patients. It should be noted, however, that the phenotypes of Q129 mice were distinct from previously generated mouse models of polyQ diseases. The Q129 mice showed myoclonus, epilepsy and progressive brain atrophy, which are the predominant clinical presentations in DRPLA patients. In contrast, feet clasping observed in R6/2 mice, SCA1 knock-in mice and DRPLA cDNA mice of AT-FL-65Q-150 (19,20,28) was absent in the Q129 mice. Electrophysiological abnormalities have been shown to vary considerably among polyQ models, even among HD yeast artificial chromosome transgenic, HD knock-in and R6/2 mice (29–31), suggesting that the synaptic dysfunctions underlying the distinct phenotypes are dependent on the promoters, copy numbers and the contexts of transgenes. Thus, the Q129 mice harboring a single copy of the full-length human *DRPLA* gene under the control of its own promoter should be highly valuable for investigating the molecular pathogenesis of DRPLA.

NIA of mutant DRPLA proteins is the essential pathophysiologic process

The regional distribution of NIA, particularly that of Q76 mice, is prominent in DRPL systems, the most vulnerable regions in DRPLA patients (1). We have also observed a similar regional distribution of NIA in human autopsied brains (10). In contrast to the Q76 mice, a massive NIA of mutant DRPLA proteins

Probe Set ID	Gene	CRE	Fold Change		Intensity-Q129	
	Neuropeptide		4W	12W	4W	12W
M88354_s_at	arginine vasopressin	●	-2.8	-8.7	0.17	0.11
M88355_s_at	oxytocin		-1.9	-5.1	0.32	0.16
X51468_f_at	somatostatin	●	-2.7	-3.0	3.45	2.55
Msa.2612.0_f_at	somatostatin	●	-2.5	-3.0	4.89	3.39
Msa.15880.0_s_at	neuropeptide Y		-1.6	-2.2	3.74	2.50
Msa.512.0_f_at	cholecystokinin	▲	-1.2	-2.0	6.87	3.96
m13227_f_at	preproenkephalin 1	●	-1.4	-1.8	3.00	2.09
	Transcriptional factor					
U29762_s_at	Dbp		-1.1	-3.2	1.28	0.54
m22326-2_s_at	Egr1	●	-1.2	-2.1	2.59	1.89
v00727_s_at	Fos	●	1.0	-2.1	0.68	0.53
x16995_s_at	Nr4a1	▲	-1.2	-2.0	1.60	1.19
Msa.3289.0_s_at	Bhlhb2	▲	-1.2	-2.0	0.76	0.67
Msa.5646.0_s_at	LIM domain only 4	▲	-1.2	-1.8	2.62	2.14
aa183623_s_at	Mef2c	▲	1.0	-1.3	2.46	1.54
aa408983_rc_g_at	Mef2d	▲	-1.0	-1.2	3.23	2.34
	Signaling molecule					
AA673405_rc_at	kalirin, RhoGEF kinase	▲	-1.6	-2.4	1.47	1.01
u05683_s_at	TYRO3 protein tyrosine kinase 3		-1.5	-2.2	1.53	0.98
Msa.1590.0_s_at	protein kinase C, delta		-1.5	-2.2	0.99	0.94
d43796_s_at	Excitatory amino acid transporter 2		1.3	-2.1	0.23	0.13
aa607353_at	Ngef (Ephexin)		-1.4	-1.9	3.45	2.21
Msa.500.0_f_at	S100 calcium binding protein A10 (calpactin)		1.2	-1.5	1.76	1.07
AB006191_at	cornichon homolog 2		-1.1	-1.4	5.54	3.81
aa245242_s_at	MARCKS-like protein		1.0	-1.3	4.81	2.16
x61432_f_at	calmodulin 1		1.1	-1.2	12.98	11.11
	Vesicular transport					
d83277_at	RAB33A, member of RAS oncogene family		-1.1	-1.8	2.29	1.18
M62418_s_at	adaptor protein complex AP-1, sigma 1	▲	-1.2	-1.5	4.61	4.07
D86214_s_at	Ca<2+>dependent activator protein for secretion		-1.1	-1.5	2.73	1.96
D83206_s_at	vesicular membrane protein p24		-1.1	-1.4	4.23	3.20
Msa.17373.0_f_at	synuclein, alpha		1.2	-1.3	1.36	1.03
	Cytoskeleton and Structual molecule					
x07215_s_at	proteolipid protein (myelin) 1		-1.0	-1.5	11.32	5.30
j04181_f_at	actin, beta, cytoplasmic		-1.1	-1.5	2.11	1.66
U19582_s_at	claudin 11	▲	1.0	-1.4	6.27	2.60
m13444_s_at	tubulin, alpha 4		-1.0	-1.4	6.14	5.34
AA590859_f_at	actin, beta, cytoplasmic		-1.0	-1.3	5.02	3.77
Msa.1236.0_f_at	thymosin, beta 4, X chromosome		1.1	-1.2	11.82	10.32
Msa.16998.0_f_at	stathmin 1		1.1	-1.2	15.32	12.45
	Cell cycle					
Msa.15616.0_s_at	cyclin D2	▲	1.1	-1.9	0.30	0.18
C78067_rc_at	Bub3	▲	1.2	-1.8	0.21	0.11
	Protein folding					
Msa.32815.0_s_at	DnaJ (Hsp40) homolog, subfamily B, member 7		1.1	-1.7	0.35	0.21
C79184_rc_s_at	karyopherin (importin) alpha 2		1.1	-1.2	4.57	3.06
	Cholesterol biosynthesis					
aa275198_s_at	HMG-CoA synthase	●	-1.1	-1.7	3.21	1.88
D29016_s_at	farnesyl diphosphate farnesyl transferase 1	▲	1.1	-1.4	1.90	1.58
	Metabolic enzyme					
Msa.34555.0_s_at	ATPase, Na+/K+ transporting, alpha 1 polypeptide	●	1.2	-4.2	0.37	0.65
Msa.3814.0_s_at	Serpinb1a		1.3	-1.9	0.39	0.18
k00811_s_at	carbonic anhydrase 2		-1.2	-1.7	5.74	4.14
	Miscellaneous					
aa289338_s_at	cAMP-regulated phosphoprotein 19	▲	-1.5	-2.5	1.22	0.90
aa409164_rc_s_at	RIKEN cDNA E130012A19 gene	▲	-1.5	-2.2	1.14	0.71
AA250009_s_at	schwannomin interacting protein 1		-1.1	-1.3	3.54	2.59

Figure 6. Expression profiles in brains of the Q129 mice compared with those in the non-TG littermates. The fold changes of the genes in the Q129 mice ($n = 3$) compared with those in the non-TG mice ($n = 3$) and the intensities in the Q129 mice at 4 or 12 weeks of age are summarized, which were calculated with the Rosetta Resolver (Ratio Experiment) using the Affymetrix-Default Ratio Builder. Fold changes are shown as columns of blue, light blue, yellow and pink indicating fold changes of < -2.0, -1.5, -1.2 and others, respectively. Filled circles: CREB targets described by Mayr and Montminy (21). Filled triangles: putative CREB targets classified as conserved CRE (22). Genes of neuropeptides in the Q129 mice, including vasopressin, oxytocin, somatostatin and neuropeptide Y, were strongly down-regulated even at 4 weeks of age. The latest description of each gene was obtained from the Probe Set at the NetAffx Analysis Center (www.affymetrix.com).

occurred throughout the Q129 mouse brain. It is noteworthy that NIA was not present on P1 even in the Q129 mice, but was the earliest change among any other abnormalities including neurological phenotypes and electrophysiological abnormalities. It should also be mentioned that the distribution of NIA far exceeded the DRPL systems. This may provide an explanation as to the controversial issue that the neuronal loss involving DRPL systems alone cannot account for the broad clinical manifestations of DRPLA. In particular, massive NIA observed in the cerebral cortex may account for the development of dementia, myoclonus and epilepsy. Taken together, these observations strongly suggest that NIA plays essential roles in the pathogenesis of DRPLA.

The mechanisms underlying the regional specificity of NIA of mutant DRPLA proteins, however, remain to be elucidated. Interestingly, NIA of mutant DRPLA proteins appeared after P4 even in the Q129 mice, whereas the transcript is abundantly expressed as early as embryonic day 5 and thereafter (32).

The postmitotic nature of neurons may underlie the age-dependent NIA of mutant DRPLA proteins starting on P4. Although further analysis is required, we speculate that regional differences in the synthesis, processing and subcellular localizations of mutant DRPLA proteins (33–35) play key roles in the region-specific distribution of NIA.

Neuronal dysfunction without neuronal loss is essential in DRPLA pathogenesis

Intriguingly, we have not observed any neuronal loss in the brains of the Q129 mice despite the progressive brain atrophy and severe neurological phenotypes. Indeed, the electrophysiological analyses demonstrated age-dependent and region-specific synaptic dysfunction along with disease progression. We demonstrated presynaptic dysfunction (altered PPRs) in PCs and pallidal neurons, and postsynaptic dysfunction (shrinkage of distal dendrites of PCs and decreased currents through AMPA and $GABA_A$ receptors in CA1 neurons). These observations strongly argue for the concept of 'neuronal dysfunction without neuronal death'. Our recent morphometric studies demonstrated marked reductions in the number and size of spines, further supporting synaptic dysfunction (14).

The concept of neuronal dysfunction without neuronal death is apparently contradictory to the neuropathological finding that neuronal loss confined to DRPL systems is the hallmark of DRPLA. As discussed above, neurological phenotypes presumably reflect neuronal dysfunction as a result of NIA, and neuronal loss may well be the latest event observed in advanced stages. Supporting this concept, juvenile-onset DRPLA patients initially do not show markedly atrophic changes in the cerebellum in magnetic resonance imaging, in contrast to markedly atrophic changes observed in late-adult-onset DRPLA patients (36).

Transcriptional dysregulations and neuronal dysfunction

In this study, we have identified genes that are down-regulated in an age-dependent manner, including those coding for neuropeptides, transcriptional factors and signaling molecules. Because of the functional relevance and strong down-regulation even at 4 weeks of age, kalirin is of particular interest, which is a multifunctional Rho guanine nucleotide exchange factor, also known as the huntingtin-associated protein interacting protein (37). The age-dependent decrease in the expression level of kalirin in the Q129 mouse brain was further confirmed by western blot analysis (Supplementary Material, Fig. S1). It has been demonstrated that the down-regulation of kalirin results in reduced linear spine density and the elimination of presynaptic endings in CA1 hippocampal neurons (38). Because the reduction in spine density is the most striking change in our morphometric analysis of Q129 mice (14), the down-regulation of kalirin might be directly involved in synaptic dysfunction. Although the functional relevance was not discussed, the down-regulation of kalirin was also observed in R6/2 mice (39; described as the expression sequence tag AA673405).

In the category of neuropeptides, arginine vasopressin showed the most striking down-regulation, which is consistent with the phenotype of central diabetes insipidus. Although clinically apparent endocrinological dysfunction has not been described in DRPLA patients, detailed investigations should be carried out on DRPLA patients, particularly on those with juvenile-onset DRPLA and highly expanded CAG repeats. Given the behavioral abnormalities observed in mice with their neuropeptides knocked out, including somatostatin (MGI:98326, impairment in motor learning) and neuropeptide Y (MGI:97374, seizure), the down-regulation of these neuropeptides may also contribute in part to the behavioral abnormalities of the Q129 mice. Dbp (MGI:2183196), Fos (MGI:95574) or excitatory amino acid transporter 2 (Slc1a2, MGI:101931) knock-out mice show seizures, suggesting that the down-regulation of these genes may also contribute to the neurological phenotypes of Q129 mice.

As shown in Figure 6, 46% of down-regulated and 61% of strongly down-regulated genes (fold change < -1.5) have CRE sites. These observations support our previous finding that CREB-dependent transcriptional activation is strongly suppressed by expanded polyQ stretches in cellular models (11,12,40). A role for CREB-mediated signaling in neurodegeneration has been provided by Mantamadiotis *et al*. (41), as determined using conditional CREB knock-out mice. They described that mice lacking both CREB and cAMP response element modulator protein (CREM) in the postnatal forebrain showed progressive neurodegeneration of the striatum and hippocampus after 1.5 months, and a neurological phenotype after 6 months, supporting the hypothesis that disruption of CREB-dependent transcription plays an essential role in neurodegeneration in polyQ diseases through transcriptional dysregulations. Although we focused on CREB-dependent transcription, it has recently been reported that expanded polyQ stretches disrupt the structures of $TAF_{II}D$ and $TAF_{II}F$ of the basal transcriptional apparatus (42). Thus, the down-regulation of genes may involve multiple mechanisms in addition to the down-regulation of CREB target genes; further investigations on the mechanisms underlying transcriptional dysregulations caused by expanded polyQ stretches should be carried out.

We should emphasize the concept of neuronal dysfunction without neuronal death as the essential pathophysiologic mechanism underlying polyQ diseases, which are associated with transcriptional dysregulations. This concept is further supported by a previous study that demonstrated the reversible recovery of phenotypic presentations in an HD mouse model after the shut-off of the expression of truncated mutant *huntingtin* (43). A recent report of deficits in experience-dependent cortical plasticity in presymptomatic HD mice (44) further strengthens this concept. This concept strongly emphasizes a wider time interval for therapeutic interventions. Because our Q129 mice closely replicate pathophysiologic processes in the human brain, as supported by the insertion of a single copy gene with its own promoter, the Q129 mice should be an ideal model for exploring possibilities for therapeutic interventions aimed at polyQ diseases.

MATERIALS AND METHODS

Generation and background of Q129 mice

Q76 transgenic mice were previously established in N1 progenies (Drm21 line) with agouti coat color that were generated from a CCE ES clone (13). Q76 mice were backcrossed to C57BL/6J, and the EF121 mosaic mouse (Q129-76) that

bred the Q129 mice (see Results) was found in the N3 generation. The EF121 mosaic mouse was also crossed with C57BL/6J females. Q129 mice used for analyses of phenotypes and expression profiling were from the N4 or N5 generation, and those used for electrophysiological analysis were from N6 or later generations. Q129 mice were established by *in vitro* fertilization using male transgenic mice at 12 weeks of age.

Brain slice preparation

Q129 transgenic mice or their age-matched non-TG littermates at either 1 to 2 weeks, 4–5 weeks or 12–15 weeks of age were decapitated under ether anesthesia. Their brains were isolated and were placed in ice-cold artificial cerebrospinal fluid (ACSF) containing NaCl (124 mM), KCl (3 mM), NaH_2PO_4 (1 mM), $MgCl_2$ (1.2 mM), $CaCl_2$ (2.4 mM) and glucose (10 mM), buffered at pH 7.4 with $NaHCO_3$ (26 mM) and saturated with 95% O_2 and 5% CO_2. The cerebellar and pallidal slices were cut parasagittally (250 μm thick) as previously described (45,46). For the preparation of hippocampal slices (250 and 400 μm thick; used for whole-cell and field recording, respectively), hippocampal formations were dissected free and cut with a tissue slicer.

Field recording

Hippocampal fEPSPs were recorded using glass electrodes (filled with ACSF) placed in the stratum radiatum of area CA1. Field EPSPs were evoked by stimulating the Schaffer collateral/commissural pathway with short current pulses (50 μs duration; 0.033 Hz) using a Teflon-coated bipolar tungsten electrode (Microprobe, Potomac, MD). LTP was induced by either one or four trains of tetanic stimulation (100 pulses/100 Hz; intertrain interval, 2 s) and monitored for 4–5 h after the tetanic stimulation to detect late-phase LTP.

Whole-cell recording

Whole-cell patch-clamp recording was made by infrared differential contrast visualization. For voltage-clamp recording in the GP and hippocampus, patch pipettes (4–6 MΩ) containing Cs-methanesulfonate (124 mM), KCl (11 mM), $MgCl_2$ (2 mM), HEPES (10 mM), Na_2-ATP (4 mM), GTP (0.3 mM), spermine (0.1 mM), QX-314 (5 mM) and 0.5% biocytin (adjusted to 280 mOsm and pH 7.3 with CsOH) were used. For recording from neurons in cerebellar nuclei, patch pipettes (4–6 MΩ) containing CsCl (30 mM), CsOH (110 mM), EGTA (1.0 mM), HEPES (10 mM), $MgCl_2$ (4.6 mM), $CaCl_2$ (0.1 mM), Na_2-ATP (4 mM) and Na_2-GTP (0.4 mM) (pH 7.3, adjusted with D-gluconate, 280 Osm, $E_{Cl} = -30$ mV) were used. For recording from PCs in the cerebellar cortex, patch pipettes (3–5 MΩ) containing CsCl (60 mM), Cs D-gluconate (10 mM), TEA-Cl (20 mM), BAPTA (20 mM), HEPES (30 mM), $MgCl_2$ (4 mM), Na_2-ATP (4 mM) and Na_2-GTP (0.4 mM) (pH 7.3, adjusted with CsOH, 280 Osm) were used.

Bicuculline methiodide (20 μM) was added to isolate glutamatergic currents. To isolate $GABA_A$ receptor-mediated currents, the NMDA receptor antagonist D(−)-2-amino-5-phosphonopentanoic acid (D-AP5, 25 μM) and the AMPA receptor antagonist 6-cyano-7-nitroquinoxaline-2,3-dione (CNQX, 10 μM) were applied to ACSF.

Immunohistochemical analysis

Q129, Q76 and non-TG littermates were anesthetized in ether and perfused with phosphate-buffered saline followed by 4% paraformaldehyde. The brains were removed and immersed in the same fixative for 16 h. Paraffin-embedded, 4-μm-thick sections were prepared and subjected to immunostaining with a rabbit polyclonal antibody against ubiquitin at 1:3200 dilution (Dako, Tokyo, Japan), the mouse monoclonal antibody 1C2 at 1:16 000 dilution (Chemicon, Temecula, CA) and goat polyclonal antibody APG840 at 1:2000 dilution as described previously (10).

RT–PCR analysis

Total RNAs were extracted from the brains (whole cerebrum and cerebellum). To avoid contamination with genomic DNA, total RNAs were extracted twice using ISOGEN (Nippon Gene, Tokyo, Japan) and converted into cDNA by priming with random hexamers using an Advantage RT-for-PCR Kit (Clontech, Mountain View, CA). PCR was performed in a 50 μl mixture containing 2.5 U AmpliTaq DNA polymerase (Applied Biosystems, Foster City, CA), 10 mM Tris–HCl (pH 8.3), 50 mM KCl, 1.5 mM $MgCl_2$, 200 μM dNTP and 5 pmol of each primer with an antisense primer labeled with FAM (5′-CTGCCCTGAGACCCCTCAAC-3′, 5′-FAM-TGGGATGGGAGAGAAGGCTG-3′). After an initial denaturation at 96°C for 2 min, PCR was performed for 30 cycles consisting of denaturation at 96°C for 45 s, annealing at 60°C for 1 min and extension at 72°C for 1 min, followed by a final extension at 72°C for 10 min. PCR products were quantified by determining the area of the chromatogram using an ABI 310 DNA sequencer and Genescan version 2.1 software (Applied Biosystems).

Western blot analysis

Brain samples from age-matched Q129, Q76 and non-TG littermates at 4, 8 and 12 weeks of age were prepared. From AT-FL-26Q-84 and AT-FL-65Q-150 mice (20), samples were obtained at 7.5 months of age; these mice were transgenic, expressing full-length DRPLA cDNAs encoding 26 and 65 CAG repeats, respectively. Sample preparation and western blot analysis were performed as described previously (17,20). Total homogenates, 20 μg per lane, and nuclear extracts, 30 and 35 μg per lane, were subjected to western blot analysis using the rabbit polyclonal antibody C580 (17), polyclonal antibody AP142 (18) and 1C2 (Chemicon), respectively.

Expression profiling analysis

Total RNAs were extracted similar to those for the RT–PCR analysis. Brain polyA(+) RNAs were prepared using an Oligotex-dT30⟨Super⟩mRNA Purification Kit (Takara, Otsu, Japan) and subjected to hybridization using Mu11KsubA and B oligonucleotide arrays (GeneChip) according to the

manufacturer's instructions (Affymetrix). Statistical analyses were performed by error-weighted ANOVA using the Rosetta Resolver gene expression data analysis system (Rosetta Biosoftware, Seattle, WA). For determining the number of dysregulated genes at 4 or 12 weeks of age, one-way ANOVA was first applied using intensity data (Time Slice). For post hoc analysis, the dysregulated genes, each of which showed both a significant difference in ratio data and an absolute fold change ≥ 1.5, were selected using the Rosetta Resolver (Ratio Experiment). For identifying the genes showing age-dependent changes, two-way ANOVA (variables: animal and time) was first applied. For post hoc analysis, genes showing a significant difference in ratio data at 12 weeks of age were selected using the Ratio Experiment. A P-value of <0.05 was considered to indicate a statistically significant difference.

SUPPLEMENTARY MATERIAL

Supplementary Material is available at *HMG* online.

ACKNOWLEDGEMENTS

We thank Satoshi Naruse, Shuichi Igarashi, Mutsuo Oyake, Hidetoshi Date, Yi Jin, Hitoshi Ichikawa, Misao Ohki, Michitoshi Watanabe, Michihiro Igarashi and Minesuke Yokoyama for helpful discussions, and Yoshitaka Yamamoto, Yoshitaka Maeda and Nobuyoshi Fujisawa for the management of laboratory animal facilities.

Conflict of Interest statement. None declared.

FUNDING

KAKENHI (Grant-in-Aid for Scientific Research) on Priority Areas (Applied Genomics and Advanced Brain Science Project), the 21st Century COE Program, Center for Integrated Brain Medical Science and Scientific Research (A) from the Ministry of Education, Culture, Sports, Science and Technology, Japan; a grant for Research for the Future Program from the Japan Society for the Promotion of Science; a grant from the Research Committee for Ataxic Diseases, the Ministry of Health, Labour and Welfare, Japan; a grant for Surveys and Research on Specific Diseases, the Ministry of Health, Labour and Welfare, Japan; the Takeda Science Foundation; the Tsubaki Memorial Neuroscience Research Foundation; and the Uehara Memorial Foundation. Funding to pay the Open Access publication charges for this article was provided by KAKENHI (Grant-in-Aid for Scientific Research) on Priority Areas (Applied Genomics).

REFERENCES

1. Naito, H. and Oyanagi, S. (1982) Familial myoclonus epilepsy and choreoathetosis: hereditary dentatorubral–pallidoluysian atrophy. *Neurology*, **32**, 798–807.
2. Takahashi, H., Ohama, E., Naito, H., Takeda, S., Nakashima, S., Makifuchi, T. and Ikuta, F. (1988) Hereditary dentatorubral–pallidoluysian atrophy: clinical and pathologic variants in a family. *Neurology*, **38**, 1065–1070.
3. Li, S.H., McInnis, M.G., Margolis, R.L., Antonarakis, S.E. and Ross, C.A. (1993) Novel triplet repeat containing genes in human brain: cloning, expression, and length polymorphisms. *Genomics*, **16**, 572–579.
4. Koide, R., Ikeuchi, T., Onodera, O., Tanaka, H., Igarashi, S., Endo, K., Takahashi, H., Kondo, R., Ishikawa, A., Hayashi, T. *et al.* (1994) Unstable expansion of CAG repeat in hereditary dentatorubral–pallidoluysian atrophy (DRPLA). *Nat. Genet.*, **6**, 9–13.
5. Nagafuchi, S., Yanagisawa, H., Sato, K., Shirayama, T., Ohsaki, E., Bundo, M., Takeda, T., Tadokoro, K., Kondo, I., Murayama, N. *et al.* (1994) Dentatorubral and pallidoluysian atrophy expansion of an unstable CAG trinucleotide on chromosome 12p. *Nat. Genet.*, **6**, 14–18.
6. Gatchel, J.R. and Zoghbi, H.Y. (2005) Diseases of unstable repeat expansion: mechanisms and common principles. *Nat. Rev. Genet.*, **6**, 743–755.
7. Davies, S.W., Turmaine, M., Cozens, B.A., DiFiglia, M., Sharp, A.H., Ross, C.A., Scherzinger, E., Wanker, E.E., Mangiarini, L. and Bates, G.P. (1997) Formation of neuronal intranuclear inclusions underlies the neurological dysfunction in mice transgenic for the HD mutation. *Cell*, **90**, 537–548.
8. Paulson, H.L., Perez, M.K., Trottier, Y., Trojanowski, J.Q., Subramony, S.H., Das, S.S., Vig, P., Mandel, J.L., Fischbeck, K.H. and Pittman, R.N. (1997) Intranuclear inclusions of expanded polyglutamine protein in spinocerebellar ataxia type 3. *Neuron*, **19**, 333–344.
9. Igarashi, S., Koide, R., Shimohata, T., Yamada, M., Hayashi, Y., Takano, H., Date, H., Oyake, M., Sato, T., Sato, A. *et al.* (1998) Suppression of aggregate formation and apoptosis by transglutaminase inhibitors in cells expressing truncated DRPLA protein with an expanded polyglutamine stretch. *Nat. Genet.*, **18**, 111–117.
10. Yamada, M., Wood, J.D., Shimohata, T., Hayashi, S., Tsuji, S., Ross, C.A. and Takahashi, H. (2001) Widespread occurrence of intranuclear atrophin-1 accumulation in the central nervous system neurons of patients with dentatorubral–pallidoluysian atrophy. *Ann. Neurol.*, **49**, 14–23.
11. Shimohata, T., Nakajima, T., Yamada, M., Uchida, C., Onodera, O., Naruse, S., Kimura, T., Koide, R., Nozaki, K., Sano, Y. *et al.* (2000) Expanded polyglutamine stretches interact with $TAF_{II}130$, interfering with CREB-dependent transcription. *Nat. Genet.*, **26**, 29–36.
12. Nucifora, F.C. Jr., Sasaki, M., Peters, M.F., Huang, H., Cooper, J.K., Yamada, M., Takahashi, H., Tsuji, S., Troncoso, J., Dawson, V.L. *et al.* (2001) Interference by huntingtin and atrophin-1 with CBP-mediated transcription leading to cellular toxicity. *Science*, **291**, 2423–2428.
13. Sato, T., Oyake, M., Nakamura, K., Nakao, K., Fukusima, Y., Onodera, O., Igarashi, S., Takano, H., Kikugawa, K., Ishida, Y. *et al.* (1999) Transgenic mice harboring a full-length human mutant *DRPLA* gene exhibit age-dependent intergenerational and somatic instabilities of CAG repeats comparable with those in DRPLA patients. *Hum. Mol. Genet.*, **8**, 99–106.
14. Sakai, K., Yamada, M., Sato, T., Yamada, M., Tsuji, S. and Takahashi, H. (2006) Neuronal atrophy and synaptic alteration in a mouse model of dentatorubral–pallidoluysian atrophy. *Brain*, **129**, 2353–2362.
15. Ikeuchi, T., Koide, R., Tanaka, H., Onodera, O., Igarashi, S., Takahashi, H., Kondo, R., Ishikawa, A., Tomoda, A., Miike, T. *et al.* (1995) Dentatorubral–pallidoluysian atrophy: clinical features are closely related to unstable expansions of trinucleotide (CAG) repeat. *Ann. Neurol.*, **37**, 769–775.
16. Llano, I., Marty, A., Armstrong, C.M. and Konnerth, A. (1991) Synaptic- and agonist-induced excitatory currents of Purkinje cells in rat cerebellar slices. *J. Physiol.*, **434**, 183–213.
17. Yazawa, I., Nukina, N., Hashida, H., Goto, J., Yamada, M. and Kanazawa, I. (1995) Abnormal gene product identified in hereditary dentatorubral–pallidoluysian atrophy (DRPLA) brain. *Nat. Genet.*, **10**, 99–103.
18. Wood, J.D., Yuan, J., Margolis, R.L., Colomer, V., Duan, K., Kushi, J., Kaminsky, Z., Kleiderlein, J.J. Jr., Sharp, A.H. and Ross, C.A. (1998) Atrophin-1, the *DRPLA* gene product, interacts with two families of WW domain-containing proteins. *Mol. Cell. Neurosci.*, **11**, 149–160.
19. Watase, K., Weeber, E.J., Xu, B., Antalffy, B., Yuva-Paylor, L., Hashimoto, K., Kano, M., Atkinson, R., Sun, Y., Armstrong, D.L. *et al.* (2002) A long CAG repeat in the mouse *Sca1* locus replicates SCA1 features and reveals the impact of protein solubility on selective neurodegeneration. *Neuron*, **34**, 905–919.
20. Schilling, G., Wood, J.D., Duan, K., Slunt, H.H., Gonzales, V., Yamada, M., Cooper, J.K., Margolis, R.L., Jenkins, N.A., Copeland, N.G. *et al.* (1999) Nuclear accumulation of truncated atrophin-1 fragments in a transgenic mouse model of DRPLA. *Neuron*, **24**, 275–286.

21. Mayr, B. and Montminy, M. (2001) Transcriptional regulation by the phosphorylation-dependent factor CREB. *Nat. Rev. Mol. Cell Biol.*, **2**, 599–609.
22. Zhang, X., Odom, D.T., Koo, S.H., Conkright, M.D., Canettieri, G., Best, J., Chen, H., Jenner, R., Herbolsheimer, E., Jacobsen, E. *et al.* (2005) Genome-wide analysis of cAMP-response element binding protein occupancy, phosphorylation, and target gene activation in human tissues. *Proc. Natl Acad. Sci. USA*, **102**, 4459–4464.
23. Myers, R.H., MacDonald, M.E., Koroshetz, W.J., Duyao, M.P., Ambrose, C.M., Taylor, S.A.M., Barnes, G., Srinidhi, J., Lin, C.S., Whaley, W.L. *et al.* (1993) *De novo* expansion of a $(CAG)_n$ repeat in sporadic Huntington's disease. *Nat. Genet.*, **5**, 168–173.
24. Goldberg, Y.P., Kremer, B., Andrew, S.E., Theilmann, J., Graham, R.K., Squitieri, F., Telenius, H., Adam, S., Sajoo, A., Starr, E. *et al.* (1993) Molecular analysis of new mutations for Huntington's disease: intermediate alleles and sex of origin effects. *Nat. Genet.*, **5**, 174–179.
25. Stevanin, G., Giunti, P., David, G., Belal, S., Dürr, A., Ruberg, M., Wood, N. and Brice, A. (1998) *De novo* expansion of intermediate alleles in spinocerebellar ataxia 7. *Hum. Mol. Genet.*, **7**, 1809–1813.
26. Koide, R., Kobayashi, S., Shimohata, T., Ikeuchi, T., Maruyama, M., Saito, M., Yamada, M., Takahashi, H. and Tsuji, S. (1999) A neurological disease caused by an expanded CAG trinucleotide repeat in the TATA-binding protein gene: a new polyglutamine disease? *Hum. Mol. Genet.*, **8**, 2047–2053.
27. Bois, P.R.J. (2003) Hypermutable minisatellites, a human affair? *Genomics*, **81**, 349–355.
28. Mangiarini, L., Sathasivam, K., Seller, M., Cozens, B., Harper, A., Hetherington, C., Lawton, M., Trottier, Y., Lehrach, H., Davies, S.W. and Bates, G.P. (1996) Exon 1 of the *HD* gene with an expanded CAG repeat is sufficient to cause a progressive neurological phenotype in transgenic mice. *Cell*, **87**, 493–506.
29. Hodgson, J.G., Agopyan, N., Gutekunst, C.A., Leavitt, B.R., LePiane, F., Singaraja, R., Smith, D.J., Bissada, N., McCutcheon, K., Nasir, J. *et al.* (1999) A YAC mouse model for Huntington's disease with full-length mutant huntingtin, cytoplasmic toxicity, and selective striatal neurodegeneration. *Neuron*, **23**, 181–192.
30. Usdin, M.T., Shelbourne, P.F., Myers, R.M. and Madison, D.V. (1999) Impaired synaptic plasticity in mice carrying the Huntington's disease mutation. *Hum. Mol. Genet.*, **8**, 839–846.
31. Murphy, K.P.S.J., Carter, R.J., Lione, L.A., Mangiarini, L., Mahal, A., Bates, G.P., Dunnett, S.B. and Morton, A.J. (2000) Abnormal synaptic plasticity and impaired spatial cognition in mice transgenic for exon 1 of the human Huntington's disease mutation. *J. Neurosci.*, **20**, 5115–5123.
32. Oyake, M., Onodera, O., Shiroishi, T., Takano, H., Takahashi, Y., Kominami, R., Moriwaki, K., Ikeuchi, T., Igarashi, S., Tanaka, H. and Tsuji, S. (1997) Molecular cloning of murine homologue dentatorubral–pallidoluysian atrophy (DRPLA) cDNA: strong conservation of a polymorphic CAG repeat in the murine gene. *Genomics*, **40**, 205–207.
33. Zhang, S., Xu, L., Lee, J. and Xu, T. (2002) *Drosophila* atrophin homolog functions as a transcriptional corepressor in multiple developmental processes. *Cell*, **108**, 45–56.
34. Sato, A., Shimohata, T., Koide, R., Takano, H., Sato, T., Oyake, M., Igarashi, S., Tanaka, K., Inuzuka, T., Nawa, H. and Tsuji, S. (1999) Adenovirus-mediated expression of mutant DRPLA proteins with expanded polyglutamine stretches in neuronally differentiated PC12 cells: preferential intranuclear aggregate formation and apoptosis. *Hum. Mol. Genet.*, **8**, 997–1006.
35. Nucifora, F.C. Jr., Ellerby, L.M., Wellington, C.L., Wood, J.D., Herring, W.J., Sawa, A., Hayden, M.R., Dawson, V.L., Dawson, T.M. and Ross, C.A. (2003) Nuclear localization of a non-caspase truncation product of atrophin-1, with an expanded polyglutamine repeat, increases cellular toxicity. *J. Biol. Chem.*, **278**, 13047–13055.
36. Koide, R., Onodera, O., Ikeuchi, T., Kondo, R., Tanaka, H., Tokiguchi, S., Tomoda, A., Miike, T., Isa, F., Beppu, H. *et al.* (1997) Atrophy of the cerebellum and brainstem in dentatorubral pallidoluysian atrophy: influence of CAG repeat size on MRI findings. *Neurology*, **49**, 1605–1612.
37. Colomer, V., Engelender, S., Sharp, A.H., Duan, K., Cooper, J.K., Lanahan, A., Lyford, G., Worley, P. and Ross, C.A. (1997) Huntingtin-associated protein 1 (HAP1) binds to a Trio-like polypeptide, with a rac1 guanine nucleotide exchange factor domain. *Hum. Mol. Genet.*, **6**, 1519–1525.
38. Ma, X.M., Huang, J., Wang, Y., Eipper, B.A. and Mains, R.E. (2003) Kalirin, a multifunctional Rho guanine nucleotide exchange factor, is necessary for maintenance of hippocampal pyramidal neuron dendrites and dendritic spines. *J. Neurosci.*, **23**, 10593–10603.
39. Luthi-Carter, R., Hanson, S.A., Strand, A.D., Bergstrom, D.A., Chun, W., Peters, N.L., Woods, A.M., Chan, E.Y., Kooperberg, C., Krainc, D. *et al.* (2002) Dysregulation of gene expression in the R6/2 model of polyglutamine disease: parallel changes in muscle and brain. *Hum. Mol. Genet.*, **11**, 1911–1926.
40. Shimohata, M., Shimohata, T., Igarashi, S., Naruse, S. and Tsuji, S. (2005) Interference of CREB-dependent transcriptional activation by expanded polyglutamine stretches—augmentation of transcriptional activation as a potential therapeutic strategy for polyglutamine diseases. *J. Neurochem.*, **93**, 654–663.
41. Mantamadiotis, T., Lemberger, T., Bleckmann, S.C., Kern, H., Kretz, O., Martin Villalba, A., Tronche, F., Kellendonk, C., Gau, D., Kapfhammer, J. *et al.* (2002) Disruption of CREB function in brain leads to neurodegeneration. *Nat. Genet.*, **31**, 47–54.
42. Zhai, W., Jeong, H., Cui, L., Krainc, D. and Tjian, R. (2005) *In vitro* analysis of huntingtin-mediated transcriptional repression reveals multiple transcription factor targets. *Cell*, **123**, 1241–1253.
43. Yamamoto, A., Lucas, J.J. and Hen, R. (2000) Reversal of neuropathology and motor dysfunction in a conditional model of Huntington's disease. *Cell*, **101**, 57–66.
44. Mazarakis, N.K., Cybulska-Klosowicz, A., Grote, H., Pang, T., Van Dellen, A., Kossut, M., Blakemore, C. and Hannan, A.J. (2005) Deficits in experience-dependent cortical plasticity and sensory-discrimination learning in presymptomatic Huntington's disease mice. *J. Neurosci.*, **25**, 3059–3066.
45. Kano, M., Hashimoto, K., Kurihara, H., Watanabe, M., Inoue, Y., Aiba, A. and Tonegawa, S. (1997) Persistent multiple climbing fiber innervation of cerebellar Purkinje cells in mice lacking mGluR1. *Neuron*, **18**, 71–79.
46. Shin, R.M., Masuda, M., Miura, M., Sano, H., Shirasawa, T., Song, W.J., Kobayashi, K. and Aosaki, T. (2003) Dopamine D4 receptor-induced postsynaptic inhibition of GABAergic currents in mouse globus pallidus neurons. *J. Neurosci.*, **23**, 11662–11672.